
ECOSYSTEM ECOLOGY

YIQI LUO, ENSHENG WENG, AND YUANHE YANG

University of Oklahoma, Norman

Ecosystem ecology is a subdiscipline of ecology that focuses on *exchange of energy and materials* between organisms and the environment. The materials that are commonly studied in ecosystem ecology include water, carbon, nitrogen, phosphorus, and other elements that organisms use as nutrients. The source of energy for most ecosystems is solar radiation. In this entry, material cycling and energy exchange are generally described before the carbon cycle is used as an example to illustrate our quantitative and theoretical understanding of ecosystem ecology.

MATERIAL CYCLING AND ENERGY EXCHANGE

Continuous exchanges of materials among compartments of an ecological system form a *cycle of elements*, usually characterized by *fluxes and pools*. Flux is a measure of the amount of materials that flows through a unit area per unit time. Pools store materials in compartments. When one ecological system is delineated with a clear boundary between inside and outside of the system, we also have to consider materials *input* into and *output* out of the system. Cycling of carbon, nitrogen, phosphorus, and other nutrient elements involves both geochemical and biological processes and is thus studied by biogeochemical approaches. In these aspects, ecosystem ecology overlaps with biogeochemistry for studying element cycles among biological and geological compartments. To fully quantify element cycles, we also need to understand *regulations* of flux, pool, input, and output by environmental factors and biogeochemical processes.

Material cycling in ecosystems is usually coupled with energy exchange. Incoming solar radiation, the source of energy for most ecosystems, is partly reflected by ecosystem surfaces and partly absorbed by plants and soil. The absorbed solar radiation is partly used to evaporate water via latent heat flux and partly converted to thermal energy to increase the temperature of ecosystem. The thermal energy is transferred to air via sensible heat flux and to soil by ground heat flux. A very small fraction of the solar radiation is converted to biochemical energy via photosynthesis.

Material and energy exchanges in ecosystem are usually described by mathematical equations. Most of the equations have been incorporated into land process models to quantitatively evaluate responses and feedback of ecosystem material and energy exchanges to global change. In this sense, quantitative analysis of ecosystem dynamics in response to global change is quite advanced. However, most of the land process models are complex and have been rarely analyzed to gain theoretical insights into ecosystem ecology.

Using the carbon cycle as an example of material and energy exchange, the following sections describe each of the major carbon cycle processes followed by their quantitative representations. Those carbon processes include leaf photosynthesis; photosynthesis at canopy, regional, and global scales; carbon transfer, storage, and release in terrestrial ecosystems; dynamics of ecosystem carbon cycling; impacts of disturbances on the carbon cycle; and effects of global change on the carbon cycle. Theoretical principles in ecosystem ecology are also presented.

Leaf Photosynthesis

The terrestrial carbon cycle usually initiates when leaf photosynthesis fixes carbon dioxide from the atmosphere into organic carbon compounds, using the energy from sunlight. Photosynthesis is vital for nearly all life on Earth directly or indirectly as the source of the energy. It is also the source of the carbon in all the organic compounds and regulates levels of oxygen and carbon dioxide in the atmosphere.

Photosynthesis begins with the light reaction when chlorophylls absorb energy from light. The light energy harvested by chlorophylls is partly stored in the form of adenosine triphosphate (ATP) and partly used to remove electrons from water. These electrons are then used in the dark reactions that convert carbon dioxide into organic compounds (i.e., carboxylation) by a sequence of reactions of the Calvin cycle. Carbon dioxide is fixed to ribulose-1, 5-bisphosphate by the enzyme in mesophyll cells, which are exposed directly to the air spaces inside the leaf. Carbon dioxide enters chlorophylls via stomata where water vapor exits the leaf. Stomatal conductance is to measure the rate of carbon dioxide influx into or water efflux from leaf.

Thus, the major processes of photosynthesis at the leaf level include light reaction, carboxylation, and stomatal conductance. Those processes can be mathematically represented by the Farquhar model for C_3 plants to calculate gross leaf CO_2 assimilation rate (A , $\mu\text{mol } CO_2 \text{ m}^{-2} \text{ s}^{-1}$)

(Farquhar et al., 1980) as

$$A = \min(J_c, J_e) - R_d, \quad (1)$$

where J_c is the rate of carboxylation with CO_2 limitation, J_e is the rate of light electron transport, and R_d is dark respiration. The leaf-level photosynthesis is determined by the one with the lowest rate of the two processes. The rate of carboxylation can be described as

$$J_c = V_m \frac{C_i - \Gamma^*}{C_i + K_C \left(1 + \frac{O_x}{K_o}\right)}. \quad (2)$$

The light electron transport process (J_e) is

$$J_e = \frac{\alpha_q \cdot I \cdot J_m}{\sqrt{J_m^2 + \alpha_q^2 \cdot I^2}} \cdot \frac{C_i - \Gamma^*}{4 \cdot (C_i + 2\Gamma^*)}, \quad (3)$$

where C_i is the leaf internal CO_2 concentration ($\mu\text{mol CO}_2 \text{ mol}^{-1}$), O_x is oxygen concentration in the air ($0.21 \text{ mol O}_2 \text{ mol}^{-1}$), V_m is the maximum carboxylation rate ($\mu\text{mol CO}_2 \text{ m}^{-2} \text{ s}^{-1}$), Γ^* is CO_2 compensation point without dark respiration ($\mu\text{mol CO}_2 \text{ mol}^{-1}$), K_c and K_o are Michaelis–Menten constants for carboxylation and oxygenation, respectively, ($\mu\text{mol CO}_2 \text{ mol}^{-1}$), I is absorbed photosynthetically active radiation (PAR, $\mu\text{mol m}^{-2} \text{ s}^{-1}$), α_q is quantum efficiency of photon capture ($\text{mol mol}^{-1} \text{ photon}$), J_m is the maximum electron transport rate ($\mu\text{mol CO}_2 \text{ m}^{-2} \text{ s}^{-1}$). Responses of leaf photosynthesis to leaf internal CO_2 concentration and radiation both follow asymptotic curves (Fig. 1)

The leaf internal CO_2 concentration, C_i , is regulated by stomatal conductance (G_s) and related to leaf photosynthesis by

$$A_n = G_s \cdot (C_a - C_i) \quad (4)$$

and

$$G_s = g_l \cdot \frac{A}{(C_i - \Gamma^*) \cdot \left(1 + \frac{D}{D_0}\right)}, \quad (5)$$

where C_a is ambient CO_2 concentration, g_l and D_0 (kPa) are empirical coefficients, and D is vapor pressure deficit (kPa). Stomatal conductance also controls water loss through leaf surface (i.e., transpiration). Since water is almost always a limiting factor for terrestrial plants, there is a tradeoff for absorbing CO_2 and reducing water loss via stomata.

Many of the photosynthetic processes are sensitive to temperature change. The temperature sensitivities of those processes are usually expressed by temperature

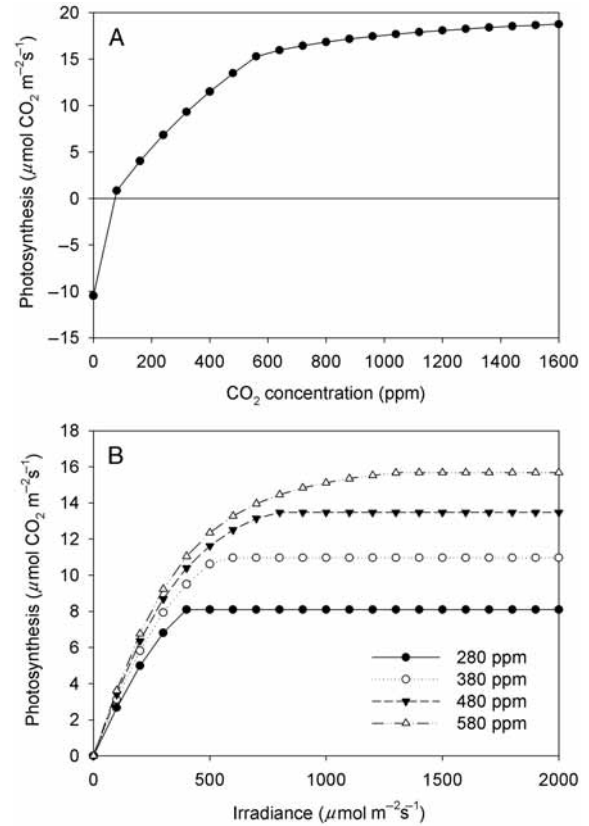


FIGURE 1 Leaf photosynthesis as a function of intercellular CO_2 concentration (A) or irradiance (B).

functions of parameters. Those parameters that are sensitive to temperature change include V_m , Γ^* , K_c , K_o , J_m , and R_d . For one given parameter, which is denoted by P , the temperature is usually expressed by Arrhenius equation as

$$P = P_{25} \cdot \exp\left(\frac{E_p \cdot (T_k - 298)}{R \cdot T_k \cdot 298}\right) \quad (6)$$

where E_p is the activation energy (J mol^{-1}) of a parameter, R is universal gas constant ($8.314 \text{ J K}^{-1} \text{ mol}^{-1}$), T_k is leaf temperature in Kelvin (K), P_{25} is the rate at 25°C . The temperature sensitivity is sometimes expressed by a peaked function to describe the increase of a process at a low temperature with a peak at an optimal temperature followed by decline (Fig. 2).

Leaf photosynthesis is also affected by nitrogen content in leaves. Leaf photosynthesis is preformed by enzymes, which require nitrogen. Most models use linear equations to relate leaf nitrogen content with maximum carboxylation, maximum electron transport, and dark respiration.

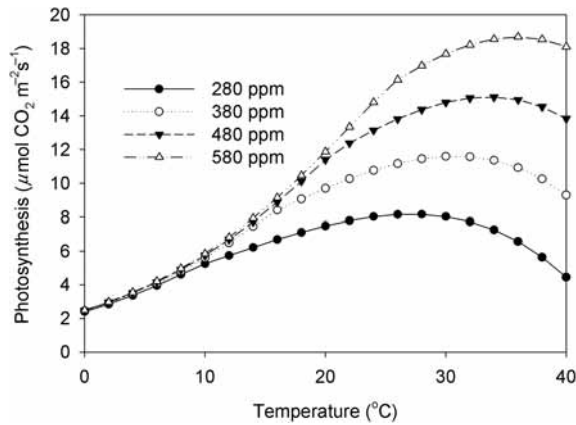


FIGURE 2 Leaf photosynthesis as a function of temperature at different CO₂ concentrations.

PHOTOSYNTHESIS AT CANOPY, REGIONAL, AND GLOBAL SCALES

When leaf photosynthesis is scaled up to the canopy level, the gradients of solar radiation, water vapor pressure, and nitrogen distribution within a canopy should be considered. The penetration of solar radiation through canopies can be described by the Beer's law as

$$I = I_0 \exp(-kL), \quad (7)$$

where I is the radiation at leaf area index L , I_0 is the solar radiation at the top of canopy, and k is light extinction coefficient. Water vapor pressure is different for the leaves within a canopy with those adjacent to bulk air. Canopies can slow down wind speed and decrease boundary layer conductance, leading to changes in the microclimate of leaves in canopies for transpiration. The photosynthetic capability as related to nitrogen concentration of the leaves is different with their positions in a canopy. Usually, nitrogen is distributed in proportion to the distribution of absorbed irradiance in canopy when there are no other limitations.

Many models have been developed to scale up photosynthesis from the leaf to canopy level based on canopy structure and gradients of environmental factors. These models can be categorized into big-leaf (single-layer) models, two-leaf models, and multiple layer models according to how canopy structure is represented and the environmental gradients are treated. The single-layer models take the whole canopy as one "big leaf," by assuming all the leaves in a canopy are the same and have the same water conditions (i.e., the humidity of air in the canopy is the same). The integration of leaf photosynthesis only considers the gradient of solar radiation. The

photosynthesis rate (carbon assimilation rate) at canopy level is thus calculated by

$$A_c = A_n \frac{1 - \exp(-kL)}{k}, \quad (8)$$

where A_c is canopy photosynthesis rate, A_n is net photosynthesis rate at leaf level.

The two-leaf models separate leaves into two classes—sunlit and shaded leaves—and thereby simulate photosynthesis in the two classes of leaves individually. The separation of sunlit and shade leaves is based on the structure of canopy and the angles of solar radiation. For the leaves in a canopy, the shade has a linear response to radiation, while the sunlit are often light saturated, and independent on irradiance, which allow averaging of solar radiation in sunlit and shaded leaves separately.

Multilayer models separate a canopy into many layers and calculate water and carbon fluxes at each layer according to its physiological properties and climatic conditions (e.g., solar radiation and water vapor). The distribution of nitrogen in canopies is often optimized for maximizing photosynthesis according to the gradient of solar radiation.

The single-layer models overestimate photosynthesis rate and transpiration. These biases caused by the big-leaf models can be corrected by adding curvature factors or tuning parameters. Single-layer models are appropriate when the details of canopy structure and its microclimate can be ignored, such as when vegetations are taken as a lower boundary of the atmosphere in global circulation models or when canopy structure is relatively simple such as tundra and desert ecosystems. Multilayer models have the flexibility to incorporate the details of canopy environmental and physiological variables. Their complexity demands high computational power for calculations and thus limits their applications at large scales. Two-leaf models can be as accurate as multilayer models but are much simpler. Therefore, they are widely used in current ecosystem and Earth system models.

Leaf and canopy photosynthesis is usually scaled up to estimate regional and global photosynthesis. There are generally two approaches to up-scaling. One is to estimate global photosynthesis from remote sensing data with a light-use efficiency constant by

$$GPP = f_{APAR} PAR \epsilon^* T_s W_s, \quad (9)$$

where PAR is photosynthetically active radiation estimated from solar radiation and f_{APAR} is the fraction of PAR that is absorbed by leaves. ϵ^* is the maximum potential light-use efficiency, and T_s and W_s are the temperature and moisture scalars, which are used to reduce the potential light-use efficiency (ϵ^*) in response to climate conditions. Another approach is to use process-based leaf and canopy photosynthesis

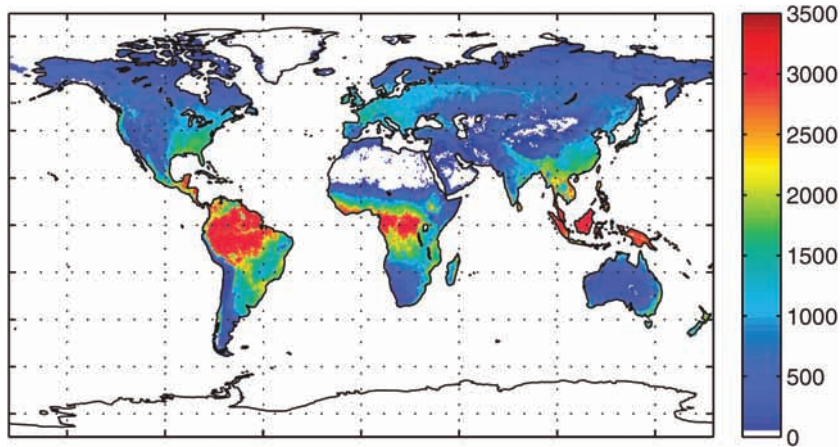


FIGURE 3 Global distribution of photosynthesis (i.e., gross primary production, GPP, Pg C year⁻¹) estimated from spatially explicit approaches. (Adapted from Beer et al., 2010, *Science* 329: 834–838.)

models such as the Farquhar model in combination of vegetation covers measured by remote sensing or simulated by models to estimate regional and global photosynthesis.

At the global scale, photosynthetic organisms convert about 120 teragrams of carbon into organic carbon compounds per year (Fig. 3). Tropical forests accounts for one-third of the global photosynthesis and have the highest photosynthetic rate per unit area. Savannahs account for about one-quarter of the global photosynthesis and are the second most important biome in terms of carbon fixation, largely due to their large area. The rate of energy capture by photosynthesis is approximately 100 terawatts, about six times larger than the power consumption of human civilization.

CARBON TRANSFER, STORAGE, AND RELEASE IN TERRESTRIAL ECOSYSTEMS

Carbohydrate synthesized from photosynthesis is partitioned for plant respiration and the growth of leaf, fine roots, and wood (Fig. 4), with small fractions to root exudates and mycorrhizae. Most large-scale models do not consider root exudation and mycorrhizae, which are usually explored by plant–soil models toward mechanistic understanding. Carbon allocation to plant respiration roughly accounts for 50% of total photosynthesis, with variation from 23% to 83% among different ecosystems. Carbon allocation between aboveground and belowground plant parts reflects the different investment of photosynthate for light harvest and uptake of water and nutrients. It varies in response to different environmental conditions. The optimal partitioning theory predicts that growth-limiting conditions usually lead to greater carbon allocation to those organs that are constrained. For instance, carbon allocation favors leaves if light becomes

more limiting and roots if plant growth is greatly limited by nutrient and water availability.

Dead leaves, stems, and roots go to litter pools and become a source of soil organic matter. The rate of litter production is determined by the turnover rates of leaves, stems, and roots. It varies with environment conditions in the short term but equals net primary production in long term. Global litter production ranges from 45 to 55 Pg C yr⁻¹, of which about 20 Pg C yr⁻¹ is from aboveground plant

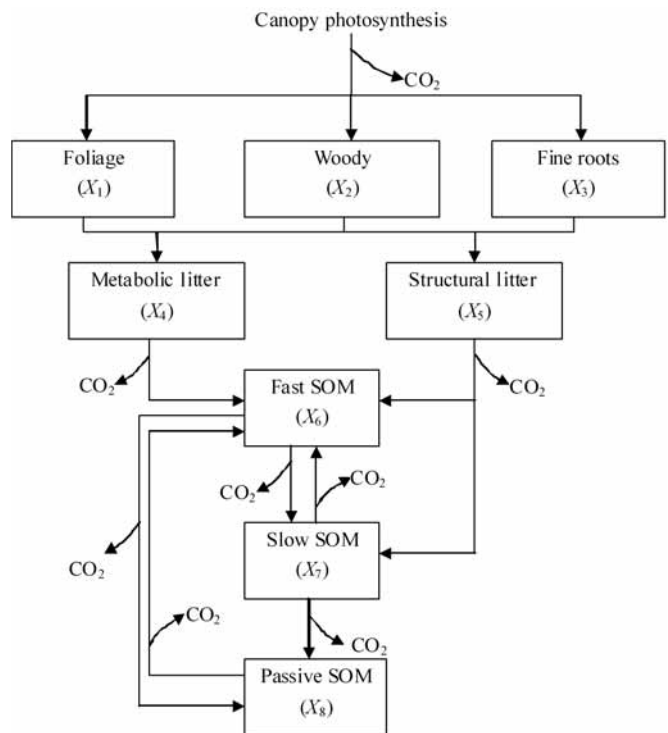


FIGURE 4 Structure of an eight-pool model to illustrate carbon pools and fluxes between them.

parts. The global litter pool is estimated at 50 to 200 Pg C. An additional 75 Pg C is estimated for the coarse woody detritus pool. Global mean steady state turnover times of litter estimated from the pool and production data range from 1.4 to 3.4 years. The mean turnover time is ~5 years for forest and woodland litter and ~13 years for coarse woody detritus. Litter is decomposed by microbes with a part respired to CO₂ and a part converted to soil organic matter.

Soil organic matter is the largest carbon pool of the terrestrial ecosystems. It receives carbon input from plants and litter and release carbon via decomposition and mineralization. Decomposition is a process conducted by microbes and affected by the quality of substrate and environmental conditions. The rate of decomposition is a key factor determining how much carbon can be stored in ecosystems. Any small changes in decomposition rate can lead to substantial changes in the carbon stock of terrestrial ecosystems, therefore affecting CO₂ concentration in atmosphere. Soil organic carbon is usually separately in conceptual models into slow and passive soil carbon pools.

The carbon processes of carbon allocation, plant growth, litter dynamics, and soil organic carbon can be mathematically represented in a matrix form:

$$\begin{cases} \frac{d}{dt} X(t) = \xi ACX(t) + BU(t), \\ X(t = 0) = X_0, \end{cases} \quad (10)$$

where $U(t)$ is the photosynthetically fixed carbon and usually estimated by canopy photosynthetic models, B is a vector of partitioning coefficients of the photosynthetically fixed carbon to plant pools (e.g., leaf, root, and woody biomass), $X(t)$ is a vector of carbon pool sizes, X_0 is a vector of initial values of the carbon pools, and A and C are carbon transfer coefficients between plant, litter, and soil pools. ξ is an environmental scalar representing effects of temperature and moisture on the carbon transfer among pools.

For a carbon cycle model as depicted in Figure 4, the vector of partitioning coefficients can be expanded to $B = (b_1 \ b_2 \ b_3 \ 0 \ 0 \ 0 \ 0 \ 0)^T$, where b_1 , b_2 , and b_3 are partitioning coefficients of photosynthetically fixed C into leaf, wood, and root, respectively.

$$C = \begin{pmatrix} 0.00258 & 0 & 0 & 0 & 0 & 0 & 0 & 0 \\ 0 & 0.0000586 & 0 & 0 & 0 & 0 & 0 & 0 \\ 0 & 0 & 0.00239 & 0 & 0 & 0 & 0 & 0 \\ 0 & 0 & 0 & 0.0109 & 0 & 0 & 0 & 0 \\ 0 & 0 & 0 & 0 & 0.00095 & 0 & 0 & 0 \\ 0 & 0 & 0 & 0 & 0 & 0.0105 & 0 & 0 \\ 0 & 0 & 0 & 0 & 0 & 0 & 0.0000995 & 0 \\ 0 & 0 & 0 & 0 & 0 & 0 & 0 & 0.0000115 \end{pmatrix}. \quad (13)$$

$X(t) = (x_1(t), x_2(t), \dots, x_8(t))^T$ is a 8×1 vector describing C pool sizes, A and C are 8×8 matrices describing transfer coefficients and given by

$$A' = \begin{pmatrix} -1 & 0 & 0 & 0 & 0 & 0 & 0 & 0 \\ 0 & -1 & 0 & 0 & 0 & 0 & 0 & 0 \\ 0 & 0 & -1 & 0 & 0 & 0 & 0 & 0 \\ f_{41} & 0 & f_{43} & -1 & 0 & 0 & 0 & 0 \\ f_{51} & f_{52} & f_{53} & 0 & -1 & 0 & 0 & 0 \\ 0 & 0 & 0 & f_{64} & f_{65} & -1 & f_{67} & f_{68} \\ 0 & 0 & 0 & 0 & f_{75} & f_{76} & -1 & 0 \\ 0 & 0 & 0 & 0 & 0 & f_{86} & f_{87} & -1 \end{pmatrix}$$

$$C = \text{diag}(c) \quad (11)$$

where f_{ij} is the transfer coefficients from pool j to pool i , $\text{diag}(c)$ denotes the diagonal matrix with diagonal components given by elements of vector $c = (c_1, c_2, \dots, c_8)^T$, and $c_j, (j = 1, 2, \dots, 8)$ represents transfer coefficients (i.e., exit rates of carbon) from the eight carbon pools $X_j, (j = 1, 2, \dots, 8)$. The initial value vector can be expanded to $X_0 = (x_1(0), x_2(0), \dots, x_8(0))^T$.

Equation 10 adequately describes most observed C processes, such as litter decomposition and soil C dynamics. It has been represented in almost all ecosystem models and integrated into Earth system models. The parameters in Equation 10 have recently been estimated from data collected in Duke Forest, North Carolina, with a data assimilation approach (Weng and Luo, 2011, *Ecological Applications*, 21: 1490–1505). Carbon transfer matrix A in Equation 10 is estimated to be

$$A = \begin{pmatrix} -1 & 0 & 0 & 0 & 0 & 0 & 0 & 0 \\ 0 & -1 & 0 & 0 & 0 & 0 & 0 & 0 \\ 0 & 0 & -1 & 0 & 0 & 0 & 0 & 0 \\ 0.9 & 0 & 0.2 & -1 & 0 & 0 & 0 & 0 \\ 0.1 & 1.0 & 0.8 & 0 & -1 & 0 & 0 & 0 \\ 0 & 0 & 0 & 0.45 & 0.275 & -1 & 0.42 & 0.45 \\ 0 & 0 & 0 & 0 & 0.275 & 0.296 & -1 & 0 \\ 0 & 0 & 0 & 0 & 0 & 0.004 & 0.01 & -1 \end{pmatrix}. \quad (12)$$

The values of the eight transfer coefficients in the diagonal matrix, $C = \text{diag}(c)$ are

The vector of partitioning coefficients B is

$$B = \begin{pmatrix} 0.14 \\ 0.26 \\ 0.14 \\ 0 \\ 0 \\ 0 \\ 0 \\ 0 \end{pmatrix}. \quad (14)$$

$U(t)$ is the C input (GPP) at time t , and its daily average over one year is estimated to be $3.370 \text{ g C day}^{-1}$. The initial values of eight pools are

$$X_0 = \begin{pmatrix} 250 \\ 4145 \\ 192 \\ 93 \\ 545 \\ 146 \\ 1585 \\ 300 \end{pmatrix}. \quad (15)$$

The environmental scalar $\xi(t)$ is a product of temperature and soil moisture response functions as

$$\xi(t) = f_W \cdot f_T, \quad (16)$$

where f_W and f_T are functions of volumetric soil moisture (W) and temperature (T), which are set to be

$$f_W = \min(0.5W, 1.0) \quad \text{and} \quad (17)$$

$$f_T = Q_{10}^{(T-10)/10}, \quad (18)$$

and Q_{10} is a temperature quotient to describe a change in decomposition rate for every 10°C difference in temperature.

PROPERTIES OF ECOSYSTEM CARBON CYCLING PROCESSES

Ecosystem carbon cycle dynamics are dictated by the properties of Equation 10, which is considered to be the governing equation of the carbon cycle in the terrestrial ecosystems. The properties of Equation 10 can be summarized in the following five aspects (see Luo and Weng, 2011). First, photosynthesis is the primary pathway of C entering an ecosystem and described by parameter $U(t)$ in Equation 10. Thus, photosynthesis determines the rate of carbon cycling in an ecosystem. In a barren soil, for

example, no carbon flows from photosynthesis to the ecosystem nor does carbon efflux or storage exist. In an ecosystem with a high rate of photosynthesis, carbon efflux is usually high. The rate of photosynthesis in an ecosystem is determined by available light, water, and nutrients, as described above.

Second, carbon in an ecosystem is compartmentalized with clear physical boundaries of different pools of C in leaf, root, wood, litter, and soil. Soil C has been further compartmentalized into conceptual or physically and chemically separable pools in some models to adequately describe its short- and long-term dynamics. Pools are represented by vector $X(t)$ with their initial values by $X(0)$ in Equation 10. Carbon influx into each of the plant pools is determined by partitioning coefficient in vector B times photosynthetic rate $U(t)$. Carbon influx to each of the litter and soil pools is determined by their donor pool sizes times exit rates of carbon from the donor pools (as represented by diagonal matrix C) times transfer coefficients in matrix A . Carbon exiting from each of the pools is described by diagonal matrix C .

Third, each of the pools has a different residence time, which is the inverse of its exit rate described by diagonal matrix C . At the ecosystem scale, the residence time measures the averaged duration of the atoms of C from the entrance via photosynthesis to the exit via respiration from the ecosystem. For individual pools, the residence time measures the averaged duration of the atoms of C from the entrance into the pool to the exit from the pool. Since each atom of C that enters an ecosystem is eventually released back to the atmosphere, residence time is a critical parameter to determine the capacity of ecosystem C storage. The residence times of the eight pools in the Duke Forest are (in units of days)

$$T = \begin{pmatrix} \tau_1 \\ \tau_2 \\ \tau_3 \\ \tau_4 \\ \tau_5 \\ \tau_6 \\ \tau_7 \\ \tau_8 \end{pmatrix} = \begin{pmatrix} 388 \\ 17,065 \\ 418 \\ 92 \\ 1053 \\ 95 \\ 10,050 \\ 86,957 \end{pmatrix}. \quad (19)$$

Thus, residence times are long in the plant wood, slow and passive soil pools. The capacity of an ecosystem to sequester C is proportional to residence times. Thus, an ecosystem sequesters more carbon if more photosynthate is partitioned to pools with long residence times, such as wood and soil. The ecosystem-scale C residence time (τ_E)

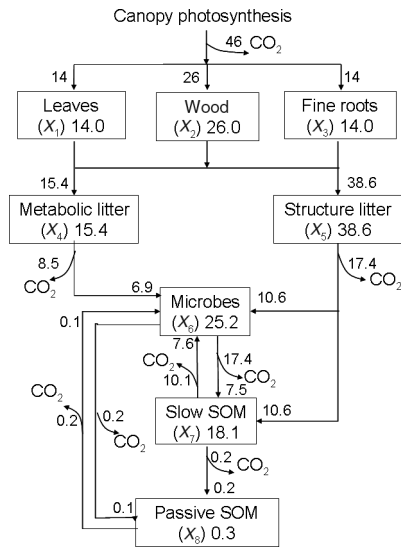


FIGURE 5 Fraction of carbon ($\times 100$) that flows through various pathways and is partitioned to the eight pools. The fraction to plant pools is determined by partitioning the coefficient in vector B in Equation 10. The fraction to litter and soil pools via each pathway is determined by the transfer coefficient matrix A . The values of vector B and matrix A are estimated from data collected in Duke Forest via data assimilation approach (Weng and Luo 2011, *Ecological Applications*, 21: 1490–1505). The fraction of carbon from photosynthesis is large to plant pools and small to soil pools, particularly to the passive soil carbon pool.

can be computed by at least two methods. One is that τ_E equals total ecosystem C content at equilibrium divided by total carbon influx. The other method is to estimate fractions of carbon entering each of the pools, which are then multiplied by the residence time of each pool. The products are summed up for all the pools. Large fractions of photosynthetically fixed carbon go to plant pools but a very small fraction to the passive soil pool (Fig. 5).

Fourth, C transfers between pools are predominantly controlled by donor pools and not much by recipient pools. C transfer from a plant to litter pool, for example, is dominated by the amount of C in the plant pool (the donor) and not the litter pool (the recipient). Although SOM decomposition is primarily mediated by microorganisms, C transfer among soil pools can be effectively modeled by proportion to donor pool sizes and not to recipient pool sizes. The donor pool-dominated transfer is the primary mechanism leading to convergence of carbon dynamics toward the equilibrium level after disturbances, as discussed below.

Fifth, decomposition of litter and soil organic matter to release CO_2 can be usually represented by a first-order decay function as described by the first term on the right side of Equation 10. Thousands of experimental studies have showed that the first-order decay function can adequately describe the mass remaining of litter with time lapsed from litter and SOM decomposition experiments

without many exceptions. The first-order decay function reinforces the property of the donor pool-dominated transfer to drive the C cycle toward equilibrium.

Mathematically, Equation 10 satisfies the Lyapunov stability conditions with negative eigenvalues of the C transfer matrix A . Using estimated parameters from the Duke Forest, the eigenvalues of matrix A in equation 10 are

$$\begin{pmatrix} -0.0106 \\ -0.0000871 \\ -0.0000115 \\ -0.0109 \\ -0.00095 \\ -0.00258 \\ -0.0000586 \\ -0.00239 \end{pmatrix}$$

According to the conditions of Lyapunov stability of a continuous linear time invariant (CLTI) system, it is stable since all the eigenvalues are negative. Model simulation also shows the convergence of ecosystem carbon storage with varied initial carbon content (Fig. 6). The carbon pool sizes at the converged equilibrium (X_{eq}) are

$$X_{eq} = \begin{pmatrix} 339 \\ 27,688 \\ 366 \\ 88 \\ 2536 \\ 113 \\ 10,020 \\ 1296 \end{pmatrix} \quad (20)$$

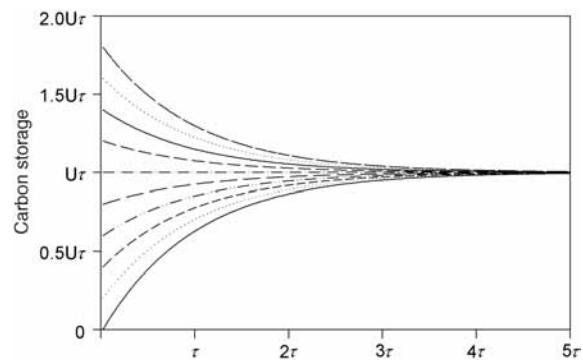


FIGURE 6 Simulated dynamics of carbon content in an ecosystem using different initial values of pools. Symbol U represents carbon influx into an ecosystem and τ the ecosystem carbon residence time. The figure illustrates the convergence of carbon storage toward the equilibrium value, which equals the product of the carbon influx (U) and residence time (τ).

Empirical evidence from many studies at the ecosystem scale has also shown that C stocks in plant and soil pools recover towards equilibrium during secondary forest succession and grassland restoration after disturbances.

DISTURBANCE EFFECTS ON THE CARBON CYCLE

An ecosystem is subject to frequent natural and anthropogenic disturbances, causing ecosystem carbon cycling processes to be in states away from equilibrium. Disturbances create disequilibrium of the carbon cycle by (1) depleting or adding carbon in pools, (2) decreasing or increasing in canopy photosynthesis, and/or (3) altering carbon residence time via changes in carbon partitioning, transfer, and decomposition.

Anthropogenic land-use conversion from forests and native grasslands to croplands, pastures, and urban areas, for example, not only results in the net release of carbon to the atmosphere, it also reduces ecosystem carbon residence time due to the elimination of carbon pools in plant wood biomass and coarse wood debris, and physical disturbance of long-term soil carbon pools. Nearly 50% of the land surface on the Earth has been used for agriculture and

domestic animal grazing, resulting in a net release of 1 to 2 Pg of carbon per year to the atmosphere (Fig. 7).

Fire removes carbon by burning live and dead plants, litter, and sometimes soil carbon in top layers. Fire often reduces ecosystem photosynthetic capacity by removing foliage biomass. It also alters physical and chemical properties of litter and soil organic matter to influence their decomposition so that carbon residence time may be affected. Globally, wildfires burn 3.5 to 4.5 million km² of land and emit 2 to 3 petagrams of carbon per year into the atmosphere (Fig. 8). Fire occurs as an episodic event, after which ecosystems usually recover in terms of photosynthetic and respiratory rates, and carbon pools in plant, litter, and soil. Ecosystem carbon processes are also affected by other episodic events like windstorms, insect epidemics, drought, and floods.

Modeling and theoretical analysis of disturbance effects on the ecosystem carbon cycle are still in their infancy. Disturbances are usually treated as prescribed events in an input file to influence biogeochemical processes, vegetation ecophysiology, species composition, age structure, height, and other ecosystem attributes. Most models then simulate recovery of plant growth, litter mass, and soil carbon. Some models consider those recovery processes

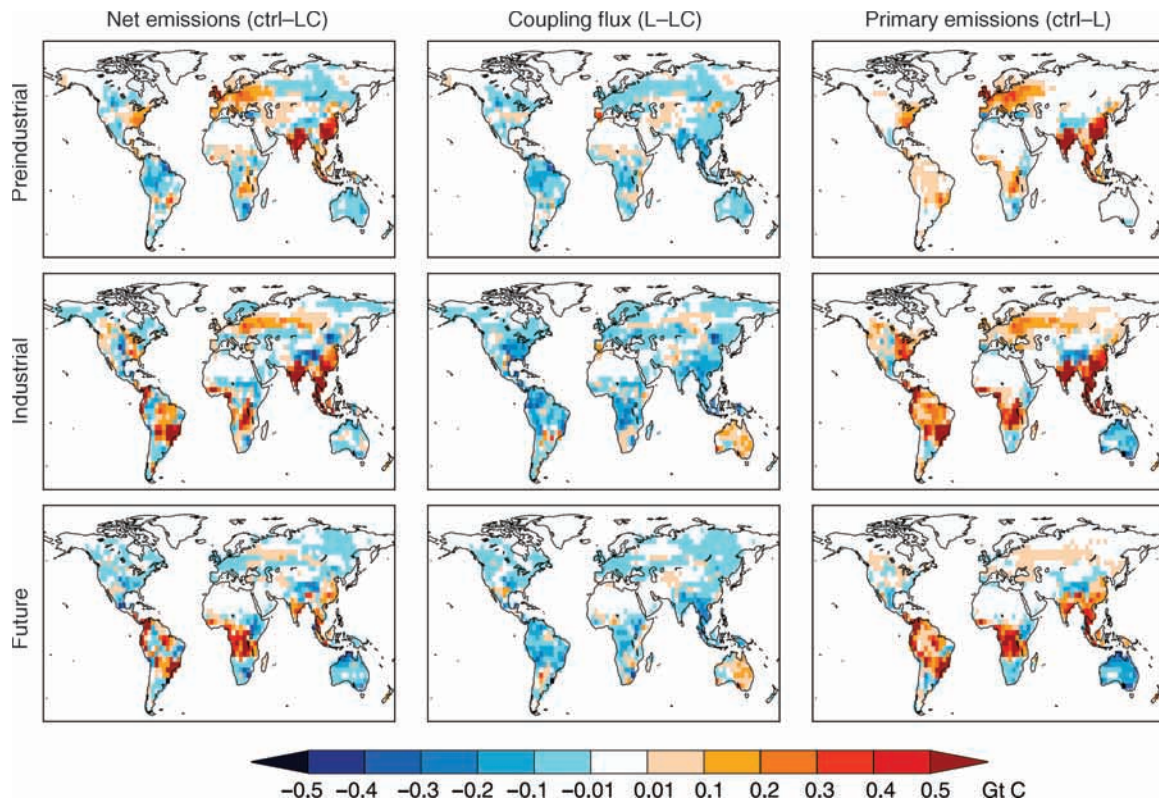


FIGURE 7 Land-use effects on carbon storage. Net emissions, coupling flux, and primary emissions of anthropogenic land cover change (ALCC) accumulated over the given time interval: preindustrial (800–1850), industrial (1850–2000), and future period (2000–2100). Units are Gt C released from each grid cell. (Adapted from Pongratz et al., 2009, *Global Biogeochemical Cycles* 23, GB4001).

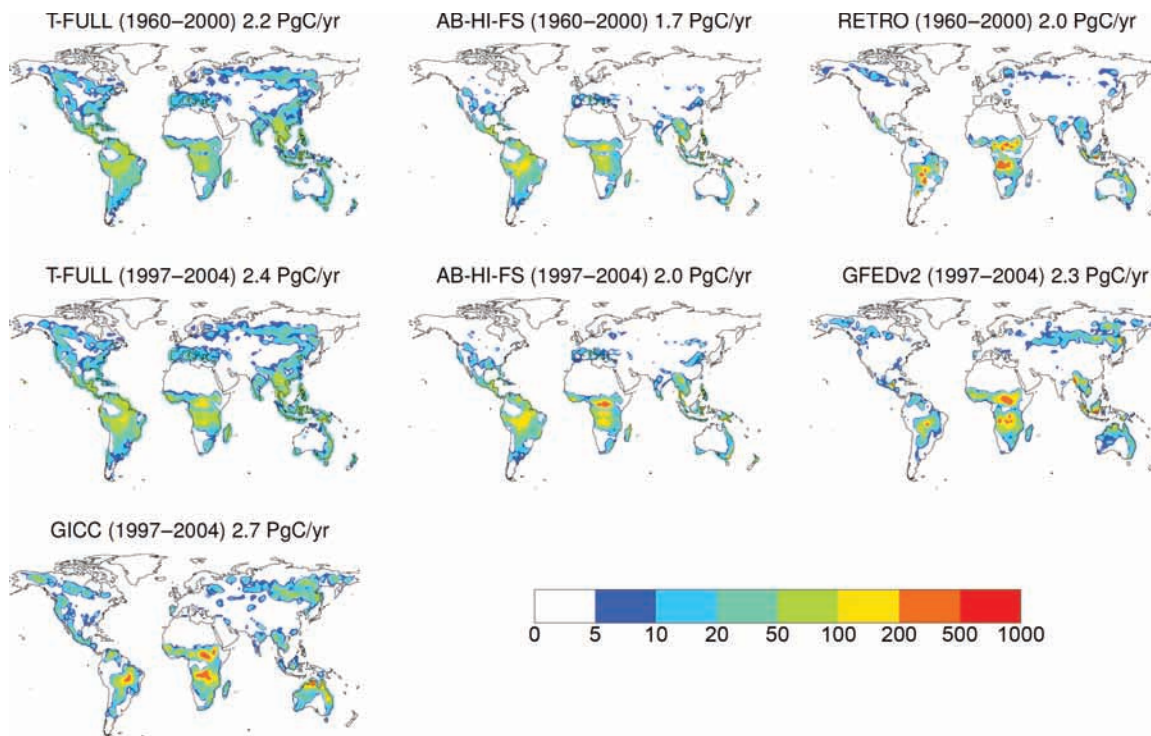


FIGURE 8 Fire effects on carbon sink. Annual mean total (wildfire plus deforestation) fire carbon emissions [$\text{g C}/\text{m}^2/\text{year}$] compared to emissions reported in other studies, including the fire products GFEDv2, RETRO, and GICC (see the original paper for description of the fire products). The model simulations are averaged over the corresponding observational periods (GFEDv2/GICC: 1997–2004; RETRO: 1960–2000). The numbers in the title of each panel are global mean fire emissions with units of PgC/year . (Adapted from Kloster et al., 2010, *Biogeosciences* 7: 1877–1902).

under the influence of global changes. However, severity of disturbances on ecosystem processes is difficult to model, largely due to the lack of data. The overall net carbon flux from forests to the atmosphere depends on the spatial extent, severity, and heterogeneity of disturbances (e.g., fire suppression, logging, and insect outbreaks). Presently, we have a limited capability of simulating the occurrences and severity of disturbances under climate change.

GLOBAL CHANGE EFFECTS ON THE ECOSYSTEM CARBON CYCLE

Many carbon cycle processes are sensitive to global change factors. For example, leaf photosynthesis is responsive to increasing atmospheric CO_2 concentration as described by the Farquhar model (Eq. 1), which creates a potential for carbon sequestration in plant biomass and soil C pools. However, growing in a high- CO_2 environment, plants may acclimate and adapt to diminish CO_2 effects. Many canopy- and ecosystem-scale processes, such as phenology, as well as nitrogen and water availability, have to be considered when we scale up leaf-level photosynthetic responses to estimate ecosystem-level responses. A meta-analysis showed that carbon and nitrogen contents in the litter and soil pools significantly increased under elevated CO_2 concentration (Fig. 9).

As global warming is happening, land surface temperature increases. While an increase in temperature usually accelerates all physical, chemical, and biological processes of ecosystems, net effects of climate warming on ecosystem carbon balance are extremely variable among ecosystems. Although instantaneous effects of temperature on leaf photosynthesis can be estimated by Equation 6, temperature affects stomatal conductance directly and indirectly via accompanied changes in vapor pressure deficit and water stresses, which further modify photosynthetic responses to climate warming. At the ecosystem scale, additional effects of temperature on photosynthetic C influx over a year is via changes in phenology and the length of the growing season under warmed climate. Similarly complex interactions of multiple processes modify responses of respiration and decomposition of litter and soil organic carbon, although temperature responses of one single processes can be usually modeled by an exponential equation as in Equation 18 or an Arrhenius equation as in Equation 6.

Human activities have also substantially altered the nitrogen cycle. As a consequence, nitrogen fertilization and deposition increase. Increased nitrogen availability usually stimulates photosynthesis and plant growth. But

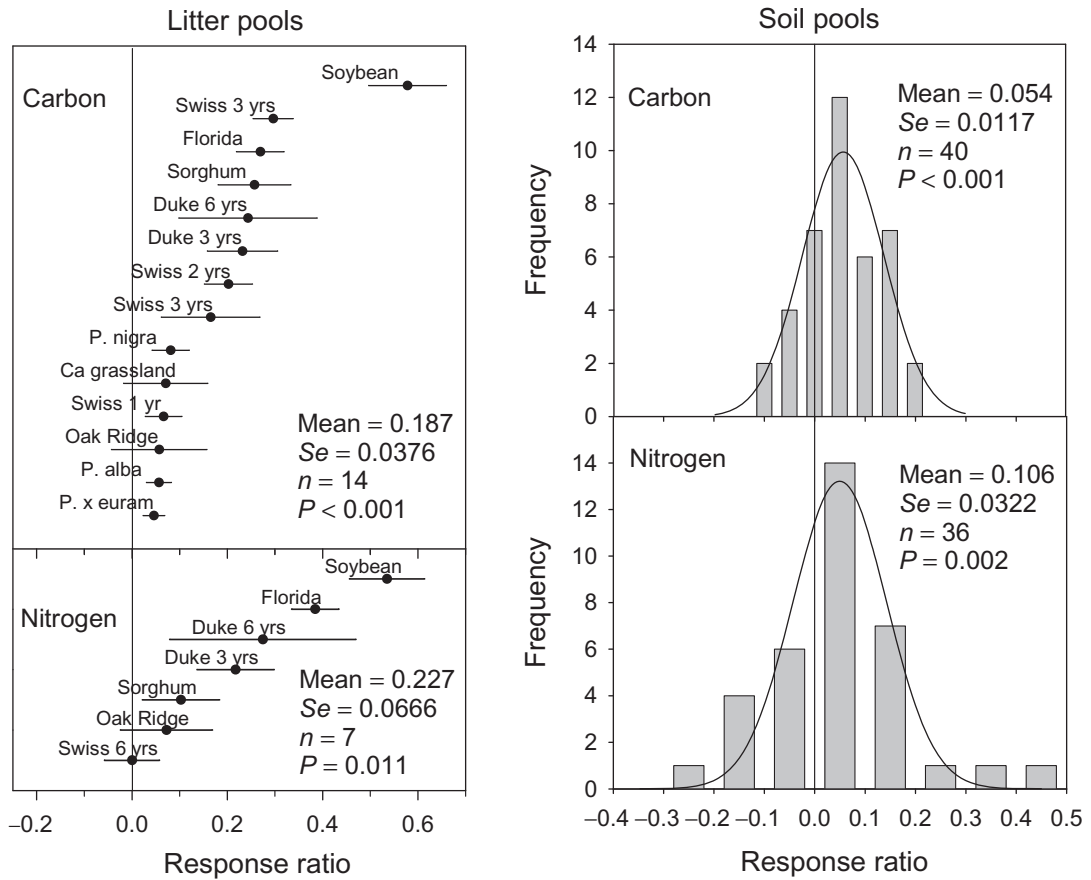


FIGURE 9 Effects of elevated CO₂ on carbon storage in litter and soil pools (Adapted from Luo et al., 2006, *Ecology* 87: 53–63.)

the increased plant growth might not lead to much net C storage in soil partly because litter produced under a high-nitrogen environment decomposes faster than that under a low-nitrogen environment and partly because nitrogen deposition or fertilization stimulate more aboveground than belowground growth, reducing C input into the soil

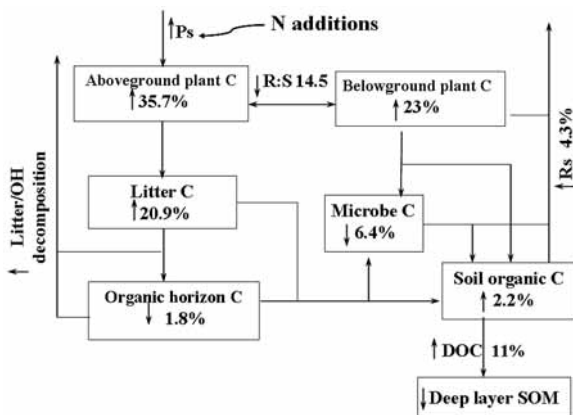


FIGURE 10 Effects of nitrogen addition on carbon storage in various plant and soil pools. (Modified from Lu et al., 2011, *Agriculture, Ecosystems and Environment*, 140: 234–244.)

(Fig. 10). Also, litter produced in the aboveground usually contributes much a smaller fraction of carbon than the belowground litter to soil carbon dynamics.

Disturbance frequency, severity, and spatial coverage (collectively called disturbance regimes) are strongly affected by global change. For example, dendrochronological and observational analyses and sedimentary charcoal records have shown tight coupling between fire activities and climate oscillations. During the mid-1980s, a period with unusually warmer springs and longer summer dry seasons, large wildfires in forests occurred more frequently in the western United States. Forest dieback and insect outbreaks usually increase in warm and dry periods. It is challenging to project future disturbance regimes in response to global change so that we can assess their impacts on the ecosystem carbon cycle.

It has long been documented that multiple states of ecosystem equilibrium exist. Natural disturbances, global change, and human intervention may trigger the state changes, resulting in major impacts on the ecosystem carbon cycle. If an ecosystem changes from a high carbon storage capacity (e.g., forest) to a new state with a low

TABLE 1
Dynamic equilibrium and disequilibrium of carbon cycle under four situations

Situation	Equilibrium	Disequilibrium
Global change	An original equilibrium can be defined at a reference condition (e.g., pre-industrial [CO ₂]) and a new equilibrium at the given set of changed conditions.	Dynamic disequilibrium occurs as C cycle shifts from the original to new equilibrium. Global change factors gradually change over time, leading to continuous dynamic disequilibrium.
Ecosystem within one disturbance–recovery episode	C cycle is at equilibrium if the ecosystem fully recovers after a disturbance. The equilibrium C storage equals the product of C influx and residence time.	C cycle is at dynamic disequilibrium and an ecosystem sequesters or releases C before the ecosystem fully recovers to the equilibrium level.
Regions with multiple disturbances over time	C cycle is at dynamic equilibrium in a region when the disturbance regime does not shift (i.e., stationary). The realizable C storage under a stationary regime is smaller than that at the equilibrium level.	C cycle is at dynamic disequilibrium and the region sequesters or releases C when the disturbance regime in the region shifts (i.e., nonstationary).
Multiple states	C cycle can be at equilibrium at the original and alternative states.	Dynamic disequilibrium occurs as an ecosystem changes from the original to alternative states.

SOURCE: Adapted from Luo and Weng 2011.

storage capacity, the ecosystem loses carbon. Conversely, a change of an ecosystem from a low to high storage capacity results in a net increase in carbon storage. For example, Amazonian forests are currently the largest tropical forests on Earth, containing 200–300 Pg C in their forests and soils. Some models have predicted that climate change could alter moist convection, leading to a reduction in dry-season rainfall in various parts of Amazonia and triggering positive feedback to state changes of the ecosystems partly to savanna. Permafrost in the high-latitude regions of the northern hemisphere contains nearly 1700 Pg of organic C. Global warming will alter physical, chemical, biological, and ecological states of the permafrost ecosystems in the region. The state change likely results in substantial C loss. State changes among multiple equilibriums can cause destabilization of the ecosystem carbon cycle. We need innovative methods to examine conditions and processes leading to the state changes.

FUTURE CARBON CYCLE DYNAMICS

Future terrestrial carbon cycle dynamics will be still governed by these processes as described by Equations 1 and 10 but strongly regulated by disturbances and global change in several ways (Table 1). First, one disturbance event causes temporal changes in carbon source and sink, followed by recovery. The recovery is driven by converging properties of ecosystem carbon processes. One disturbance event may not have much impact on the long-term carbon cycle unless disturbance regimes shift. Second, shifts in disturbance regimes are usually caused by global change and human intervention. Disturbance regime shifts can result in substantial changes in the long-term carbon cycle over regions. Third, global change can directly

alter C influx and residence time, leading to changes in the carbon cycle. Global change can also indirectly affect the carbon cycle via changes in ecosystem structure and disturbance regimes. Fourth, when ecosystem structure changes and disturbance regimes shift, the ecosystem carbon cycle might move to alternative states. State changes among multiple equilibriums can have the most profound impact on future land carbon cycle dynamics, especially if they happen at regions with large carbon reserves at risk.

SEE ALSO THE FOLLOWING ARTICLES

Biogeochemistry and Nutrient Cycles / Environmental Heterogeneity and Plants / Gas and Energy Fluxes across Landscapes / Regime Shifts

FURTHER READING

- Bolker, B. M., S. W. Pacala, and W. J. Parton. 1998. Linear analysis of soil decomposition: insights from Century model. *Ecological Applications* 8: 425–439.
- Bonan, G. B. 2008. Forests and climate change: forcings, feedbacks, and the climate benefits of forests. *Science* 320: 1444–1446.
- Chapin, F. S., III, P. A. Matson, and H. A. Mooney. 2002. *Principles of terrestrial ecosystem ecology*. New York: Springer.
- Farquhar, G. D., S. von Caemmerer, and J. A. Berry. 1980. A biochemical model of photosynthetic CO₂ assimilation in leaves of C₃ species. *Planta* 149: 78–90.
- Luo, Y. Q., and E. S. Weng. 2011. Dynamic disequilibrium of terrestrial carbon cycle under global change. *Trends in Ecology & Evolution* 26: 96–104.
- Parton, W. J., D. S. Schimel, C. V. Cole, and D. S. Ojima. 1987. Analysis of factors controlling soil organic-matter levels in Great-Plains grasslands. *Soil Science Society of America Journal* 51: 1173–1179.
- Potter, C. S., J. T. Randerson, C. B. Field, P. A. Matson, P. M. Vitousek, H. A. Mooney, and S. A. Klooster. 1993. Terrestrial ecosystem production: a process model-based on global satellite and surface data. *Global Biogeochemical Cycles* 7: 811–841.
- Schlesinger, W. H. 1997. *Biogeochemistry: an analysis of global change*, 2nd ed. San Diego: Academic Press.
- Sellers, P. J., R. E. Dickinson, D. A. Randall, A. K. Betts, F. G. Hall, J. A. Berry, G. J. Collatz, A. S. Denning, H. A. Mooney, C. A. Nobre, N. Sato, C. B. Field, and A. Henderson-Sellers. Modeling the exchange of energy, water, and carbon between continents and the atmosphere. *Science* 275: 502–509.